CASL-U-2015-0159-000

The Implementation and Analysis of the MOC and CMFD Adjoint Capabilities in the 2D-1D Code MPACT

Ang Zhu, Yunlin Xu, Thomas Saller, and Thomas Downar
University of Michigan

April 19, 2015

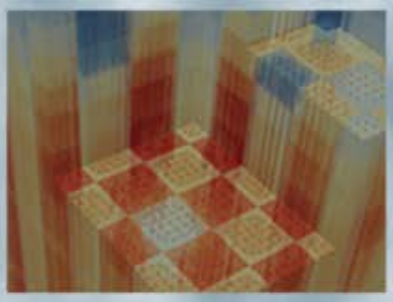

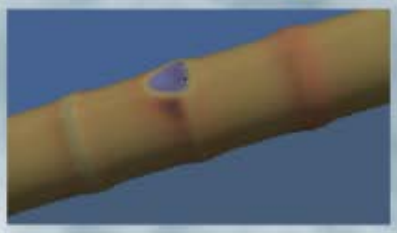

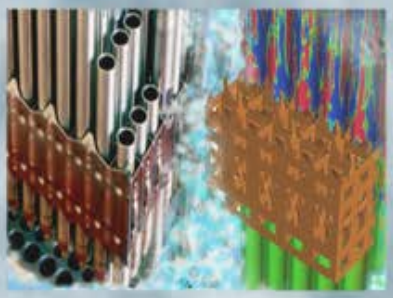

U.S. DEPARTMENT OF ENERGY | Nuclear Energy
CASL-U-2015-0159-000

ANS MC2015 - Joint International Conference on Mathematics and Computation (M&C), Supercomputing in Nuclear Applications (SNA) and the Monte Carlo (MC) Method • Nashville, TN • April 19-23, 2015, on CD-ROM, American Nuclear Society, LaGrange Park, IL (2015)

THE IMPLEMENTATION AND ANALYSIS OF THE MOC AND CMFD ADJOINT CAPABILITIES IN THE 2D-1D CODE MPACT

Ang Zhu, Yunlin Xu, Thomas Saller and Thomas Downar
Department of Nuclear Engineering & Radiological Science
University of Michigan, Ann Arbor, 48105, USA
angzhu@umich.edu; yunlin@umich.edu; tgsaller@umich.edu;
downar@umich.edu

ABSTRACT

The objective of the work presented in this paper was to develop both the Method of Characteristics (MOC) and Coarse Mesh Finite Difference (CMFD) adjoint capabilities within the framework of the pin resolved, 2D-1D method in the core transport neutronics code MPACT. The first section of this paper provides a description of the algorithms developed in MPACT to solve the adjoint flux for both the MOC and CMFD equations. The computational complexity and efficiency of the MOC based and CMFD based adjoint flux calculations are then compared, and numerical results are presented. The MOC and CMFD adjoint flux solutions are compared for a simple pin cell case which shows good agreement in the non-resonance energy region. This suggests that the use of the CMFD-based adjoint flux is sufficiently accurate for cases in which pin-resolution is not important such as core reactivity edits. A SPERT transient rod assembly case is then used to compare MPACT spatial transient results to the Exact Point Kinetic Equation (EPKE) results using the CMFD adjoint flux. Good agreement is observed between the EPKE and the MPACT spatial transient results which provides confidence in CMFD adjoint flux calculation for practical core reactivity edits in MPACT.

Key Words: MOC, CMFD, Adjoint Calculation, Transient, MPACT

1 INTRODUCTION

MPACT [1, 2] is a three-dimensional (3-D) whole core transport code being developed jointly at the University of Michigan and Oak Ridge National Laboratory (ORNL) as part of the DOE CASL reactor simulation hub. MPACT is capable of generating pin resolved power distributions using integral transport solutions to the heterogeneous reactor problem in which the actual pin-resolved geometrical configuration of fuel components such as the pellet and cladding is explicitly retained during the flux solution. The cross section data needed for the neutron transport calculation are obtained directly from a multi-group microscopic cross section library similar to those used in lattice physics codes. Hence MPACT involves neither a priori homogenization nor group condensation for the core spatial solution.

The steady state integral transport solution is obtained by the method of characteristics (MOC) that employs discrete ray tracing. Since the direct application of MOC to a full 3-D core a configuration requires considerable amounts of memory and computing time for practical reactor applications, an alternative approximate 3-D solution method was implemented in MPACT based on a 2-D/1-D approach, which employs planar MOC solutions within the framework of the 3-D coarse mesh finite difference (CMFD) formulation [3]. The axial coupling is resolved by one-dimensional (1-D) lower order solutions and the planar and axial problems are coupled through transverse leakage. The use of a lower order 1-D solution in the axial direction

is justified by the fact that most heterogeneity in the core occurs in the radial direction rather than the axial. Several 1D nodal methods are currently available in MPACT to solve the axial problem, including diffusion, SN, and SPN kernels.

A pin-resolved transient capability was recently designed and implemented in MPACT [4]. As part of the development of the transient capability in MPACT, the adjoint capability was developed primarily to provide the ability to perform reactivity edits for practical reactor applications. Both an MOC and CMFD based adjoint flux capability was implemented in MPACT and the first section of this paper provides a description of the MOC and CMFD adjoint equations and solution algorithms. The second section provides numerical result for comparison between CMFD and MOC based adjoint flux and comparison of MPACT results to EPKE results.

2 THE MOC AND CMFD ADJOINT METHODS

The fundamental mode adjoint neutron flux has always been useful in reactor physics for the treatment of perturbations of eigenvalue problems. The adjoint flux provides a convenient method to estimate the perturbed eigenvalue without exactly solving the often very complicated perturbed systems [5]. One of the important perturbations for practical neutron transport applications is the insertion of reactivity, where the change of material composition, temperature, etc. will either increase or decrease the eigenvalue of the system.

The MOC based adjoint flux calculation was previously implemented in MPACT in order to generate the asymptotic diffusion coefficient [6]. Because of the computational complexity of the MOC based adjoint flux, the CMFD based adjoint flux calculation capability was also designed and implemented in MPACT with the intention to accurately approximate the MOC based adjoint flux for practical reactor core applications.

As described in the reference [5], the adjoint operation is defined by the scalar product Eq. (1) to hold for all allowed $\mathbf{\Psi}$ and $\mathbf{\Phi}$ of all functional space, where and $\mathbf{H}^*$ is the adjoint operator of $\mathbf{H}$ and <> is the operation to integrate over all spaces:

$$<\mathbf{\Psi},\mathbf{H\Phi}>=<\mathbf{H}^*\mathbf{\Psi},\mathbf{\Phi}>=<\mathbf{\Phi},\mathbf{H}^*\mathbf{\Psi}> \tag{1}$$

The following sections will first develop the MOC based and then the CMFD based adjoint equations that were implemented in MPACT.

2.1 MOC Adjoint Equations

For simplicity, the development of the MOC-based adjoint can be most easily demonstrated using the 1-D isotropic scattering transport equation. The forward equation is shown in Eq. (2).

$$\begin{aligned}&\mu\frac{\partial\psi(x,\mu,E)}{\partial x}+\Sigma_t(x,E)\psi(x,\mu,E)\\&=\frac{1}{2}\int_0^\infty\int_{-1}^1\Sigma_s(x,E'\to E)\psi(x,\mu',E')d\mu'dE'+\frac{\chi(x,E)}{2}\int_0^\infty\int_{-1}^1\nu\Sigma_f(x,E')\psi(x,\mu',E')d\mu'dE'\end{aligned} \tag{2}$$

where $\psi(x,\mu,E)$ is the angular flux and the other terms are the standard reactor physics notations. Using the definition of adjoint operator in Eq. (1), the adjoint form of Eq. (2) can be easily written as:

$$
\begin{aligned}
&-\mu\frac{\partial\psi^*(x,\mu,E)}{\partial x}+\Sigma_t(x,E)\psi^*(x,\mu,E)\\
&=\frac{1}{2}\int_0^\infty\int_{-1}^{1}\Sigma_s(x,E\to E')\psi^*(x,\mu',E')d\mu'dE'+\frac{\nu\Sigma_f(x,E)}{2}\int_0^\infty\int_{-1}^{1}\chi(E')\psi^*(x,\mu',E')d\mu'dE'
\end{aligned}
\tag{3}
$$

In order to solve the forward flux Eq. (2), the energy domain is discretized using the multigroup approximation:

$$
\begin{aligned}
&\mu\frac{\partial\psi_g(x,\mu)}{\partial x}+\Sigma_{t,g}(x)\psi_g(x,\mu)\\
&=\frac{1}{2}\sum_{g'=1}^{G}\int_{-1}^{1}\Sigma_{s,g'\to g}(x)\psi_{g'}(x,\mu)d\mu'+\frac{\chi_g(x)}{2}\sum_{g'=1}^{G}\int_{-1}^{1}\nu\Sigma_{f,g'}(x)\psi_{g'}(x,\mu)d\mu'
\end{aligned}
\tag{4}
$$

The corresponding adjoint equation to Eq. (4) can then be written as:

$$
\begin{aligned}
&-\mu\frac{\partial\psi_g^*(x,\mu)}{\partial x}+\Sigma_{t,g}(x)\psi_g^*(x,\mu)\\
&=\frac{1}{2}\sum_{g'=1}^{G}\int_{-1}^{1}\Sigma_{s,g\to g'}(x)\psi_{g'}^*(x,\mu')d\mu'+\frac{\nu\Sigma_{f,g}(x)}{2}\sum_{g'=1}^{G}\int_{-1}^{1}\chi_{g'}(x)\psi_{g'}^*(x,\mu')d\mu'
\end{aligned}
\tag{5}
$$

Using the convenient variable change $\psi_g^*(x,\mu)=\hat{\psi}_g(x,-\mu)$ and then setting $\mu=-\mu$, Eq. (5) becomes Eq. (6) which is a similar form to the forward MOC Eq. (4), where only the scattering matrix is reversed and nu-fission is exchanged with the fission spectrum.

$$
\begin{aligned}
&\mu\frac{\partial\hat{\psi}_g(x,\mu)}{\partial x}+\Sigma_{t,g}(x)\hat{\psi}_g(x,\mu)\\
&=\frac{1}{2}\sum_{g'=1}^{G}\int_{-1}^{1}\Sigma_{s,g\to g'}(x)\hat{\psi}_{g'}(x,\mu')d\mu'+\frac{\nu\Sigma_{f,g}(x)}{2}\sum_{g'=1}^{G}\int_{-1}^{1}\chi_{g'}(x)\hat{\psi}_{g'}(x,\mu')d\mu'
\end{aligned}
\tag{6}
$$

The algorithm used for solving the forward equation can then be used to solve the corresponding adjoint equation. One important fact should be noted is that the adjoint transport equation is not technically solved since that would require multigroup cross sections obtained by flux-weighting with adjoint fluxes. Instead, only the adjoint of the multigroup transport equation is solved here.

2.2 CMFD Adjoint Equations

CMFD acceleration method has been widely used to reduce the computational burden for steady state and transient reactor simulations. The balance equation for each neutronics node is coupled to its neighboring nodes through the interface neutron currents:

$$
\sum_{u=x,y,z}\frac{1}{h_u}\left(\bar{J}_{gur}-\bar{J}_{gul}\right)+\Sigma_{rg}\phi_g-\sum_{\substack{g'=1\\g'\neq g}}^{G}\Sigma_{gg'}\phi_{g'}=\frac{\chi_g\sum_{g'=1}^{G}\nu\Sigma_{fg'}\phi_{g'}}{k_{eff}}
\tag{7}
$$

where h, J, $\Sigma_{rg}^{m}, \phi_{g}^{m}$ are the node length, current in the surface, removal cross-section, and scalar flux using standard reactor notations. The "r" and "l" subscripts refer to the left and right nodes.

In order to preserve the higher order solution, a $\hat{D}_S$ term is added to the diffusion term as shown in Eq. (8):

$$\bar{J}_s^{CMFD} = -\tilde{D}_S(\phi_R - \phi_L) + \hat{D}_S(\phi_R + \phi_L) \tag{8}$$

where $\tilde{D}_S = \dfrac{2D_r D_l}{h_l D_r + h_r D_l}$, which comes from the standard diffusion theory using Fick's law.

The $\hat{D}_S$ term is calculated using Eq. (9) based on the solution of higher order equations (e.g. MOC, NEM and SN):

$$\hat{D}_S = \frac{\bar{J}_s^{local} + \tilde{D}_S(\phi_R - \phi_L)}{(\phi_R + \phi_L)} \tag{9}$$

Using Eq. (8) in Eq. (7), set of equations can be formulated with only the average scalar flux as unknowns. This can be written in the usual matrix form as:

$$\mathbf{A}\phi = \frac{\mathbf{F}\phi}{k_{eff}} \tag{10}$$

where **A** and **F** matrix are the left hand side and right hand side of Eq. (7) respectively.

Eq. (10) can be solved by the standard power iteration, where in each iteration either group sweeping or a direct matrix inversion can be used to determine the solution of the inner iteration fixed source problem $\mathbf{A}x=b$.

As shown in the references [5], the transpose of a matrix satisfies the definition of the adjoint operation defined in Eq. (1). As a result, the CMFD adjoint equation can be expressed as:

$$\mathbf{A}^*\phi^* = \frac{\mathbf{F}^*\phi^*}{k_{eff}^*} \tag{11}$$

where the fundamental mode forward and adjoint eigenvalues are identical.

The matrix **A** is explicitly constructed and stored during the forward CMFD solve in MPACT and the transpose operation is simply performed by the intrinsic transpose subroutine provided by PETSc [7]. The fission source operator **F** term is not constructed explicitly, but rather can be written in matrix form in Eq. (12), and the transpose operation can be performed by simply switching the fission spectrum and fission cross section vector as shown in Eq. (13).

$$\mathbf{F} = \boldsymbol{\chi}\upsilon\boldsymbol{\Sigma}_{\mathbf{f}} \tag{12}$$

$$\mathbf{F}^* = \upsilon\boldsymbol{\Sigma}_{\mathbf{f}}^*\boldsymbol{\chi}^* \tag{13}$$

Eq. (11) can also be solved using the power iteration, which is the same procedure to solve the forward CMFD equation. Since the matrix **A** and **F** are fixed for the given problem, there is no need to update them during the power iteration. In addition, the majority of the right hand side term can be shifted to the left hand side, and the method is well known as Wielandt Eigenvalue Shift.

2.3 Comparison of Computational Cost of the CMFD and MOC Adjoint Calculation

Apart from possible differences in the accuracy of the CMFD and MOC based adjoint flux, the CMFD adjoint flux has two major computational advantages over the MOC adjoint flux. First there is the obvious saving in FLOP count because the CMFD adjoint flux calculation is much less computationally intensive and requires less than 10% of the forward MOC calculation time for most applications. The second computational advantage is because all the coefficients of the adjoint CMFD matrix are calculated and stored during the forward calculation while some of the MOC coefficients required for the adjoint solution would need to be evaluated on the MOC mesh during the forward calculation, such as the difference in the leakage term $\Omega\nabla\psi$ when Eq. (18) is used to evaluate the dynamic reactivity. This would increase the memory usage as well as increase coding complexity.

3 NUMERICAL RESULTS

3.1 Comparison of CMFD and MOC Adjoint Flux

A typical PWR pin cell case was created to examine the differences in CMFD and MOC based adjoint flux solution. The CMFD and MOC based adjoint flux are shown in Figure 1, where the MOC adjoint flux is homogenized by flat source region volume and both CMFD and MOC adjoint flux are normalized. These two sets of adjoint fluxes agree very well in the non-resonance groups (Group one is the fastest group), while some discrepancies are observed in the resonance energy groups.

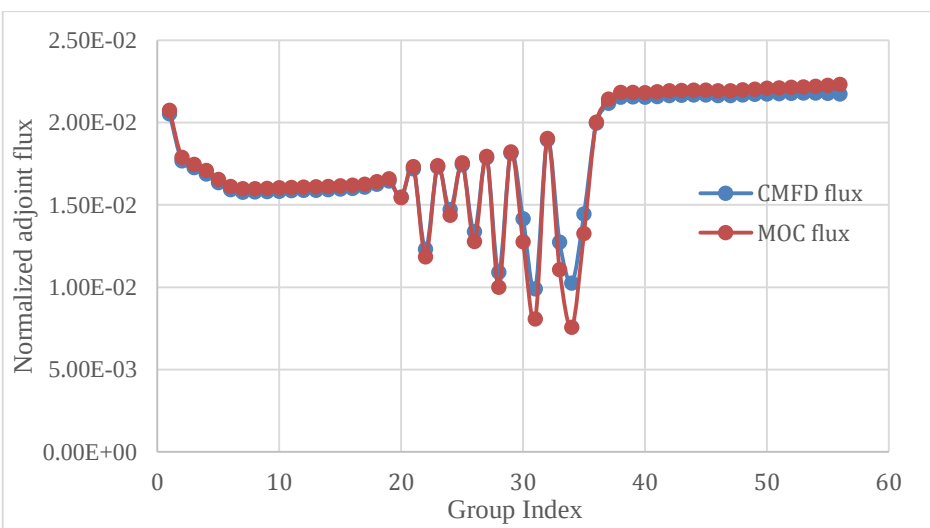

Figure 1 MOC and CMFD based adjoint flux for a pin cell

The MOC based region-wise adjoint flux is shown in Figure 2, where the inner rings have much less neutron importance than the outer rings primarily due to self-shielding effects. For example, adjoint solution suggests that the outermost ring has more than 50 times more importance than the innermost ring for group 34. The large radial distribution of the MOC based adjoint flux can explain the difference between MOC and CMFD adjoint flux.

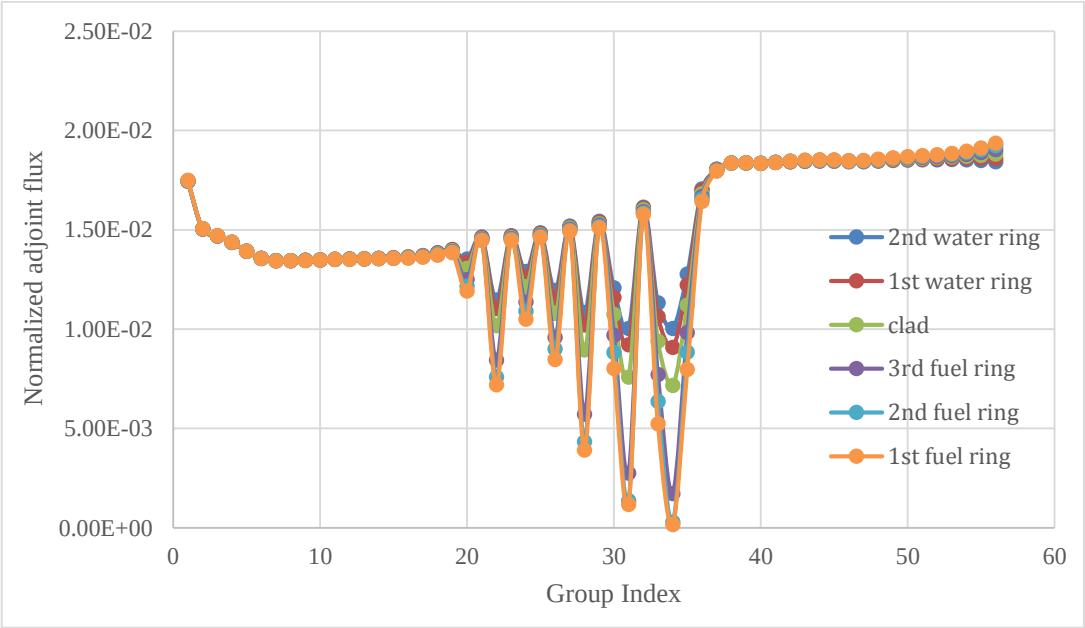

Figure 2 MOC based adjoint flux for radial subregions

However, these differences in the pin-resolved adjoint solution are likely not crucial to most practical reactor core applications. Unlike the forward fluxes, the primary purpose of the adjoint flux is to provide an evaluation of the "importance" of the forward flux, and thus the discrepancy between CMFD and MOC should be less significant in predicting core wise parameters such as the coefficients for the EPKE.

3.2 Comparison of SPERT transient rod assembly results with Exact Point Kinetic Equation

In order to verify the accuracy of the CMFD adjoint flux calculation and point kinetics parameter edits, the MPACT transient results were compared to EPKE.

The point kinetic parameters edits capability was implemented using the CMFD adjoint flux as the weighting function and their accuracy is crucial to the EPKE results. The EPKE is formulated based on the fact that the flux solution can be separated into an amplitude and a shape function:

$$\phi_g(\mathbf{r},t) = p(t)\psi_g(\mathbf{r},t) \tag{14}$$

where ϕ_g is the CMFD flux and $p(t)$, $\psi_g(\mathbf{r},t)$ represent amplitude and shape functions respectively. One constrain for this separation is to maintain the integration of the shape function to be a constant:

$$<\phi_g^*(\mathbf{r})\frac{1}{v_g(\mathbf{r})}\psi_g(\mathbf{r},0)> = <\phi_g^*(\mathbf{r})\frac{1}{v_g(\mathbf{r})}\psi_g(\mathbf{r},t)> \tag{15}$$

The EPKE is defined in Eq. (16) and Eq. (17) and the derivation can be found in [8]:

$$\frac{dp(t)}{dt} = \frac{\rho(t)-\beta^{eff}(t)}{\Lambda(t)}p(t) + \frac{1}{\Lambda_0}\sum_k \lambda_k(t)\zeta_k(t) \tag{16}$$

$$\frac{d\zeta_k(t)}{dt} = \frac{\Lambda_0}{\Lambda(t)}\beta_k^{eff}(t)p(t) - \lambda_k(t)\zeta_k(t),\ k=1,2...,6 \tag{17}$$

The point kinetics parameter reactivity, delay neutron fractions, neutron generation time and delay neutron constants are defined in Eq. (18) to Eq. (21) respectively:

$$\rho(t) = \frac{<\phi^*(r)\left(\frac{\mathbf{F}}{k_{eff}} - \mathbf{A}\right)\phi(r,t)>}{<\phi_g^*(\mathbf{r})\chi_g(\mathbf{r})S^F(\mathbf{r},t)>} \tag{18}$$

$$\beta_k^{eff}(t) = \frac{<\phi_g^*(\mathbf{r})\chi_{dk,g}(\mathbf{r})\beta_k(\mathbf{r})S^F(\mathbf{r},t)>}{<\phi_g^*(\mathbf{r})\chi_g(\mathbf{r})S^F(\mathbf{r},t)>}, k=1,2...,6 \quad \beta^{eff}(t) = \sum_k \beta_k^{eff}(t) \tag{19}$$

$$\Lambda(t) = \frac{<\phi_g^*(\mathbf{r})\frac{1}{v_g(\mathbf{r})}\phi_g(\mathbf{r},t)>}{<\phi_g^*(\mathbf{r})\chi_g(\mathbf{r})S^F(\mathbf{r},t)>} \tag{20}$$

$$\lambda_k(t) = \frac{<\phi_g^*(\mathbf{r})\lambda_k(\mathbf{r})\chi_{dk,g}(\mathbf{r})C_k(\mathbf{r},t)>}{<\phi_g^*(\mathbf{r})\chi_{dk,g}(\mathbf{r})C_k(\mathbf{r},t)>} \tag{21}$$

where $S^F(\mathbf{r},t) = \frac{1}{k_{eff}}\sum_{g'}\nu\Sigma_{f,g'}(\mathbf{r},t)\phi_{g'}(\mathbf{r},t)$, is the total fission source and the matrix operators in Eq. (18) are the same used in Eq. (10).

The *p(t)* function in Eq. (16) is an amplitude function and it has different numerical value and physical meaning to the core power calculated by MPACT transient solver, as a result a power norm factor for EPKE is requited:

$$f_{fp}(t) = \frac{<\kappa\Sigma_{fg}(r,t)\phi_g(r,t)>\ p(0)}{p(t)<\kappa\Sigma_{fg}(r,0)\phi_g(r,0)>} = \frac{<\kappa\Sigma_{fg}(r,t)\psi_g(r,t)>}{<\kappa\Sigma_{fg}(r,0)\psi_g(r,0)>},\ f_{fp}(0)=1 \tag{22}$$

The final fission power level of EPKE is calculated by Eq. (23) with $p(t)$ predicted by Eq. (16):

$$H(t) = f_{fp}(t)p(t) \tag{23}$$

The iteration schemes for both MPACT and EPKE are shown in Figure 3. The point kinetics parameters are edited after MOC solve at each transient step and fed into EPKE solver. The EPKE is then solved using the point kinetics parameters at each time step and same time discretization scheme of MPACT transient solver is applied, which includes implicit Euler discretization for $dp(t)/dt$ term in Eq. (16) and second order approximation for power when precursor equations are integrated in Eq. (17). The TH feedback in MPACT transient solver is included in the point kinetics parameters, so there is no explicated TH feedback in the EPKE model.

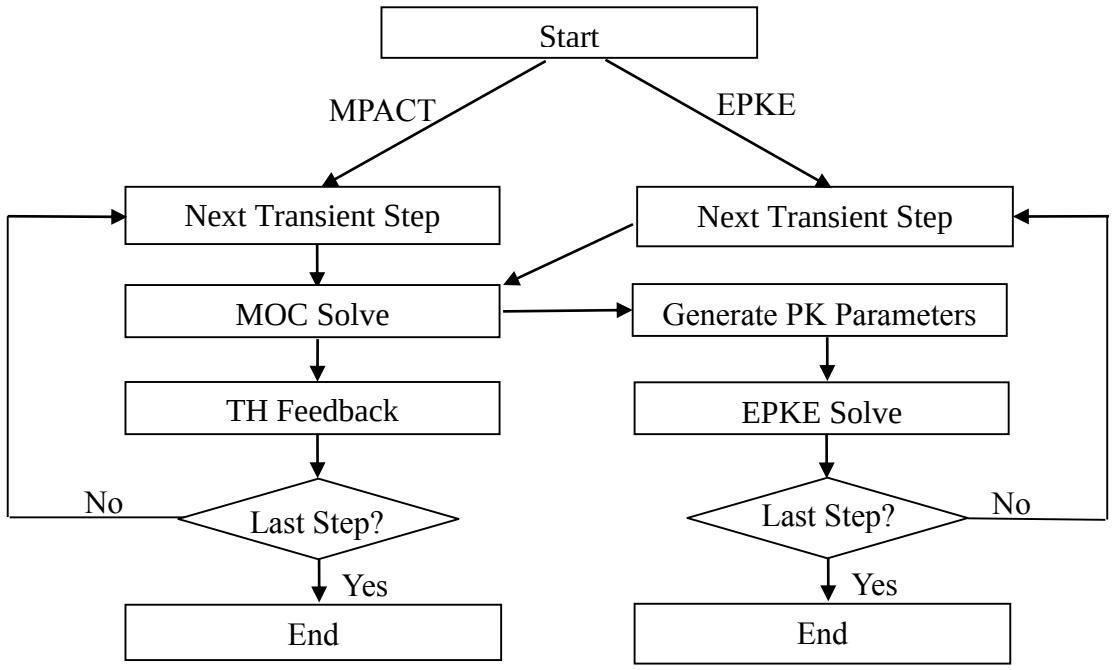

Figure 3 Iteration scheme for MPACT transient solver and EPKE solver

The test problem is a SPERT transient rod assembly, which is adopted from the whole core SPERT simulation [4]. The geometry of SPERT core is shown in Figure 3 and radial layout of the transient rod assembly is presented in Figure 4. The transient rod assembly has 4 by 4 pins radially and 120 cm height with 20 axially layers. The transient blade is withdrawn in 0.08 seconds and a 5ms time step was used for the whole trainset simulation. The transient solver developed in [4] is coupled with an internal thermal-hydraulics module in MPACT which solves transient mass and energy equations and the whole core power and coolant mass flow rate were adjusted to take into account the fact that only one assembly was simulated. The MPACT transient simulation of this problem required approximately 1 hour using 20 cores with 2.4GHz AMD processors.

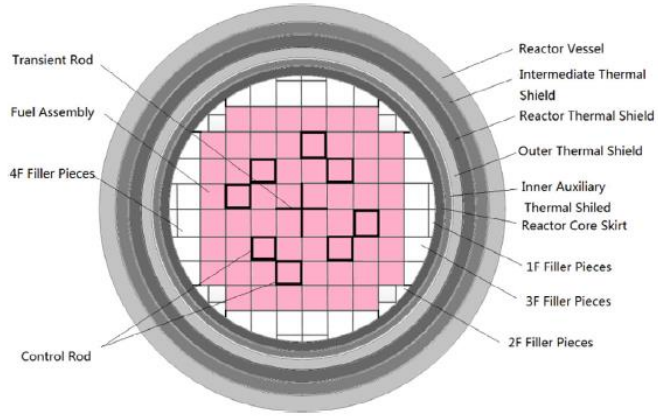

Figure 4 SPERT III E-Core Cross [9]

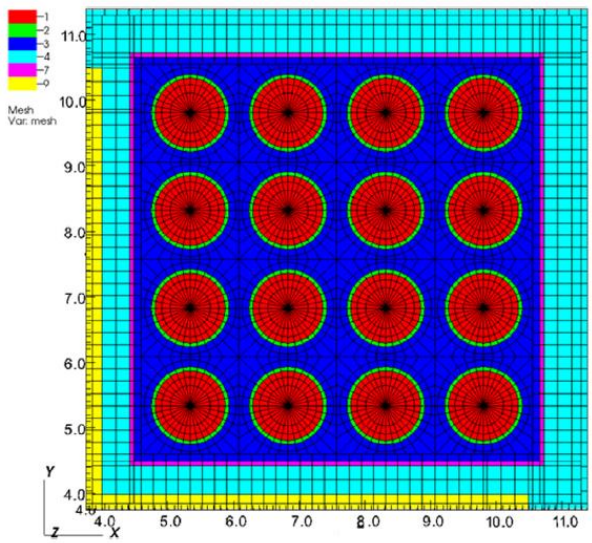

Figure 5 MPACT model of 16-rod assembly with cruciform transient rod [9]

The power histories for both MPACT spatial transient solver and EPKE solver are shown in Figure 6 and maximum relative error shown in Figure 7is smaller than 3.5E-4. The results provide confidence in the application of the CMFD adjoint calculation to practical reactor applications for editing dynamic point kinetics parameters.

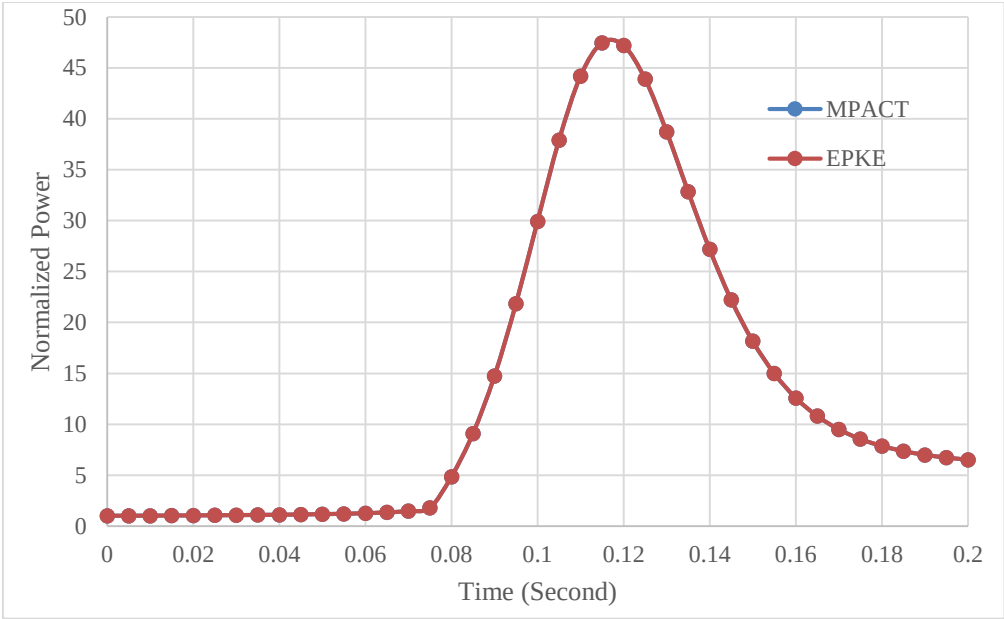

Figure 6 SPERT transient rod assembly power history

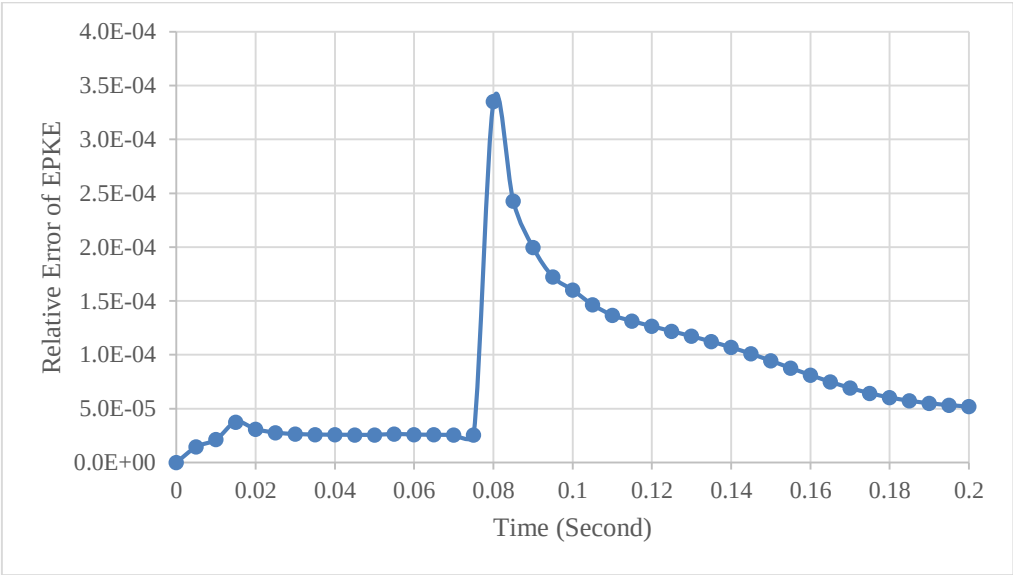

Figure 7 Relative error of EPKE compared to MPACT for SPERT transient rod assembly

4 SUMMARY AND CONCLUSIONS

The paper presented the development and validation of the MOC and CMFD based adjoint capabilities within the framework of the pin resolved, 2D-1D method in the core neutronics code MPACT. The first section of this paper provided a description of the adjoint algorithms developed and implemented in MPACT. The 1-D isotropic transport formula was first used to present the algorithm to solve the multigroup MOC based adjoint flux. The standard CMFD

formulation was then used to develop the CMFD adjoint flux algorithm. A comparison between MOC based and CMFD based adjoint flux calculation was then provided regarding computational efficiency and coding complexity.

In the second section of the paper, numerical results were presented for application of the adjoint flux in MPACT. At first the comparison for the MOC and CMFD adjoint flux calculated by a pin cell case were shown, and the results agreed well in the non-resonance energy region. This suggested that the use of the CMFD adjoint flux was sufficiently accurate for core reactivity edits. Then MPACT transient result of a SPERT transient rod assembly was then compared to the solution of Exact Point Kinetic Equation (EPKE), which was based on the point kinetic parameters generated by the MPACT CMFD adjoint flux. Good agreement was observed between EPKE and the MPACT results from a SPERT transient rod assembly case, which provided confidence in CMFD adjoint flux calculations for the core reactivity edits during practical reactor transient applications.

Currently work is ongoing to validate the transient capability in MPACT using the SPERT E-Core rod ejection experiments [4]. The adjoint capability in MPACT is essential to the analysis of the MPACT results for these experiments. Future work within CASL will be to apply the transient capability within MPACT to a several challenge problems involving full core LWR applications. The adjoint flux capability developed here has the potential to assist in the understanding of the computational results.

5 ACKNOWLEDGMENTS

This research was supported by the Consortium for Advanced Simulation of Light Water Reactors (www.casl.gov), an Energy Innovation Hub (http://www.energy.gov/hubs) for Modeling and Simulation of Nuclear Reactors under U.S. Department of Energy Contract No. DE-AC05-00OR22725.

6 REFERENCES

1. MPACT Team, MPACT Theory Manual, Version 1.0 , University of Michigan, Ann Arbor, MI, October, 2013.
2. B. Kochunas, et al, “Overview of Development and Design of MPACT: Michigan Parallel Characteristics Transport Code”, Proc. Int. Conf. Mathematics and Computational Methods Applied to Nuclear Science & Engineering (M&C 2013), American Nuclear Society, Sun Valley, ID, USA, May 5-9, [CD-ROM] (2013)
3. B. Kelly and E. Larsen, “2D/1D Approximations to the 3D Neutron Transport Equation: Theory,” International Conference on Mathematics and Computational Methods Applied to Nuclear Science & Engineering (M&C 2013) Sun Valley, Idaho, USA, May 5-9, 2013
4. A. Zhu, et al, “Transient Methods For Pin-Resolved Whole Core Transport Using The 2d-1d Methodology In Mpact”, Joint International Conference on Mathematics and Computation (M&C), Supercomputing in Nuclear Applications (SNA) and the Monte Carlo (MC) Method

(M&C 2015), American Nuclear Society, Nashville, TN, USA, April 19-23, [CD-ROM] (2015)

5. K. Ott, R. Neuhold. Introductory nuclear reactor dynamics[M]. La Grange Park: American Nuclear Society, 1985.
6. T. Travis and E. Larsen, "An Asymptotic, Homogenized, Anisotropic, Multigroup Diffusion Approximation to The Neutron Transport Equation", Proc. Int. Conf. The Role of Reactor Physics toward a Sustainable Future (PHYSOR2014), American Nuclear Society, Kyoto, Japan , September 28-October 3, [CD-ROM] (2014)
7. S. Balay, et al. PETSc Users Manual Revision 3.4[J]. 2013.
8. T. Downar, Y. Xu, V. Seker, PARCS v3.0 U.S. NRC Core Neutronics Simulator User/Theory Manual, Department of Nuclear Engineering and Radiological Sciences University of Michigan, Ann Arbor, MI, September 2009.
9. L. Cao, et al., "Neutronics Modeling of the SPERT III E-Core Critical Experiments with MPACT and KENO," *Annals of Nuclear Energy*, **80** (2015) 207–218